Electronic Supplementary Information

Correlation of Micellar Structures with Surface-Plasmon-Coupled Fluorescence in a Strategy for Fluorescence Enhancement

Ki-Se Kim,[a] Hun Kim,[b] Jeong-Hee Kim,[a] Jin-Hyung Kim,[a] Chang-Lyoul Lee,[c] Frédéric Laquai,[b]

Seong Il Yoo*[d] and Byeong-Hyeok Sohn*[a]

[a] *Department of Chemistry, Seoul National University, Seoul, 151-747, Korea. Email: bhsohn@snu.ac.kr; Tel: +82-2-883-2154; Fax: +82-2-889-1568*

[b] *Max-Planck-Institute for Polymer Research, Ackermannweg 10, D-55128 Mainz, Germany.*

[c] *Advanced Photonic Research Institute (APRI), Gwangju Institute of Science and Technology (GIST), 1 Oryong-dong, Buk-gu, Gwanju 500-712, Korea.*

[d] *Department of Polymer Engineering, Pukyong National University, Busan 608-739, Korea. Email: siyoo@pknu.ac.kr*

Time-dependent extinction spectra of Ag NPs

To monitor the growth of Ag NPs, 2 mL of solution was extracted from the reaction vessel and then immediately cooled down in an ice bath. At early stage of growth (up to 5 min), the extinction intensity is quite weak, indicating incomplete reduction of Ag+ by citrate ions. However, the extinction intensity increased with reaction time and then saturated after around 30 min. In addition, the peak position was shifted from ~ 415 nm to ~ 430 nm with reaction time and then maintained. Since these observations imply the complete reaction of Ag NPs, we selected this condition for the synthesis of Ag NPs.

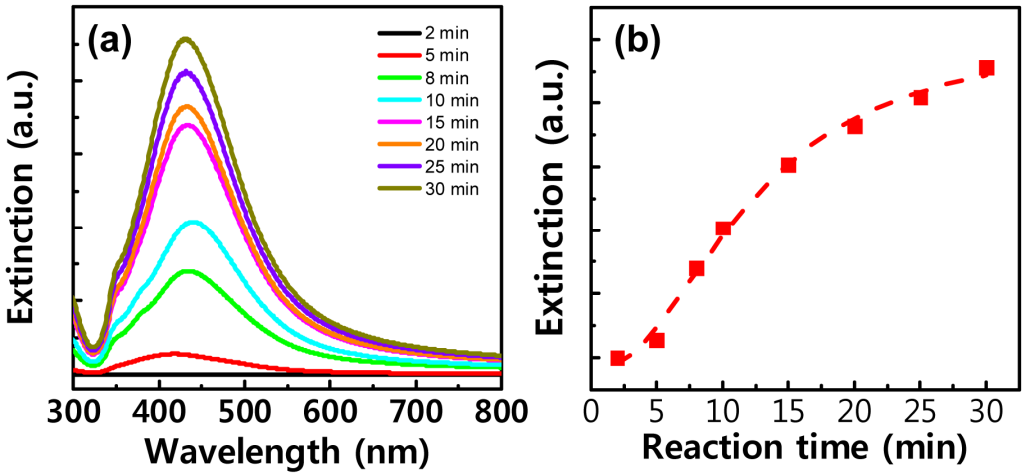

Figure S1. The changes of extinction spectra (a) and the peak intensity at 430 nm (b) of Ag NPs at different reaction times.

TEM image of Ag NPs

For a TEM sample, an aliquot of a solution of Ag NPs was dropped on a carbon-coated TEM grid and then dried at ambient condition.

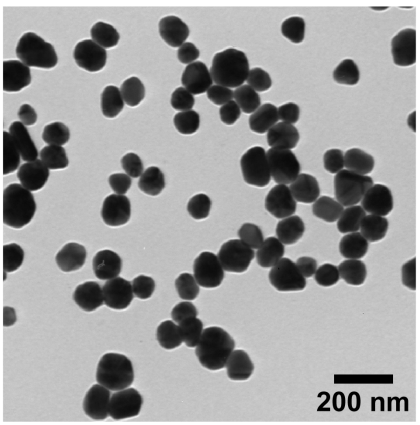

Figure S2. TEM image of citrate-stabilized Ag NPs.

Extinction spectra of Ag NPs

The extinction spectra of Ag NPs vary in a solution and thin film state. For instance, the extinction spectrum of Ag NPs in an aqueous solution has a maximum around 430 nm (Figure S3a), while that of the same Ag NPs coated on the quartz substrate was blue-shifted to ~ 400 nm (Figure S3b). This behavior can be understood by the decrease in the refractive index (n) of the surroundings (n = 1.33 for water and n = 1.0 for air). In order to confirm the uniform deposition of Ag NPs, we measured the extinction intensity of Ag NPs on the quartz substrates and it was nearly identical at each preparation time. In addition, after coating PS-PVP micelles on the NP substrate, the peak position was further shifted to ~ 454 nm (Figure S3c) because of the higher refractive index of PS coronas (n = 1.59).

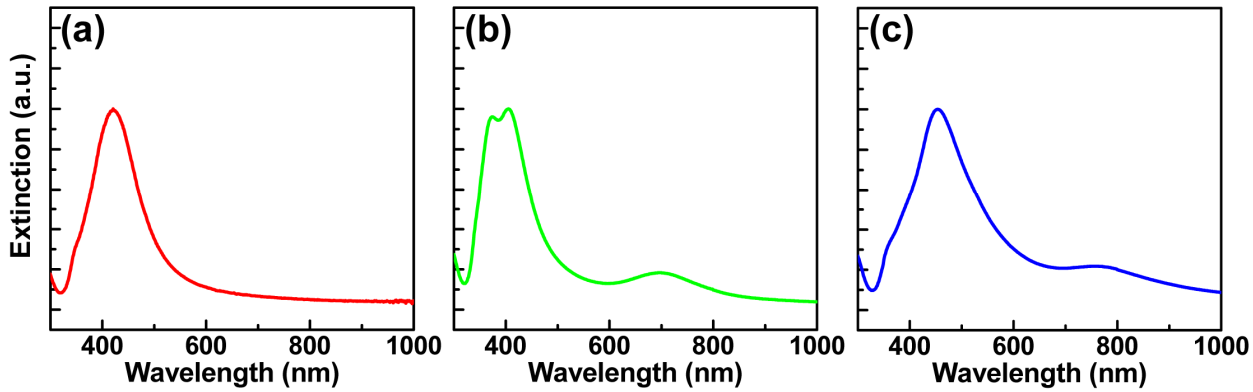

Figure S3. Extinction spectra of Ag NPs. (a) in aqueous solution; (b) on quartz substrate; (c) after being coated by PS-PVP micelles.

X-ray photoelectron spectra (XPS)

To verify whether the surface of Ag NPs was coated by PS-PVP micelles, XPS spectra of Ag (3d) photoelectron peak were compared before (black line) and after (red line) being coating by PS-PVP micelles (Figure S4). While the clear decrease in the intensity of Ag peak strongly indicates that the NP surface was covered by PS-PVP micelles, the resident Ag peak implies that the NP surface was not fully coated by the micelles. Since the formation of a micellar film can be driven by the lateral assembly of micelles, i.e., by a lateral capillary force, the presence of the curved NP surface may interrupt the capillary action to prevent the full coverage of the NP surface.

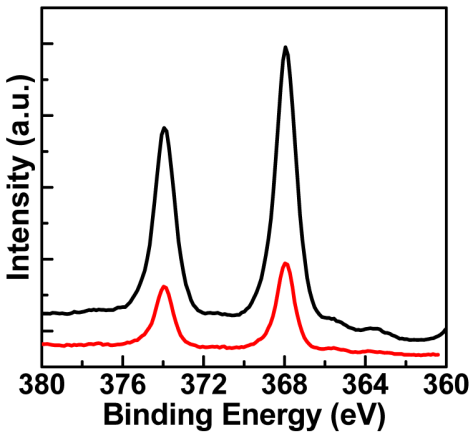

Figure S4. X-ray photoelectron spectra of Ag peak before (black) and after (red) being coating by PS-PVP micelles.

Time components of TRF spectrum

The decay of fluorescence intensity (I(t)) can be modeled as the sum of individual exponentials that is described by[1]

$$I(\mathrm{t}) = \sum_i \alpha_i \exp(-t/\tau_i) \text{ ---------- (S1)}$$

where τ_i are the individual lifetimes and α_i are the amplitudes. Here, we normalized the values of α_i to $\sum_i \alpha_i = 1$, so the average lifetime of the dyes can be obtained by $\tau_{ave} = \sum_i \alpha_i \tau_i$. After fitting the TRF results in Figure 2 and 4 with the multiexponential Eq. (S1), the amplitude (α_i), lifetime (τ_i), and average lifetime (τ_{ave}) of the dyes on bare and NP substrates were calculated and summarized in Table S1 and S2.

samples	α_1 (%)	τ_1 (ns)	α_2 (%)	τ_2 (ns)	τ_{ave}(ns)
R123 (bare substrate)	74	1.22	26	3.64	1.84
R123 (NP substrate)	72	0.36	28	1.61	0.71
S101 (bare substrate)	62	0.64	38	2.17	1.21
S101 (NP substrate)	78	0.25	22	1.14	0.45

Table S1. Time components obtained from micelles containing R123 or micelles containing S101 on the bare and NP substrates, i.e., from Figure 2d and 2h.

samples	α_1 (%)	τ_1 (ns)	α_2 (%)	τ_2 (ns)	τ_{ave} (ns)
R123 (bare substrate)	73	1.28	27	3.69	1.93
R123 (NP substrate)	74	0.25	26	1.68	0.63
S101 (bare substrate)	52	0.42	48	2.31	1.33
S101 (NP substrate)	77	0.18	23	1.55	0.49

Table S2. Time components obtained from mixed micelles containing R123 and S101 on the bare and NP substrates, i.e., from Figure 3d and 3e.

Efficiency of non-radiative energy transfer process

To examine the quenching effect by non-radiative energy transfer to metal NPs, we calculated the quenching efficiency (E_{NET}) according to a recent empirical equation[2]

$$E_{NET} = 1 - \frac{1}{1 + (d_0 / d)^4} \quad \text{---------- (S2)}$$

where d_0 is the characteristic distance at which 50 % quenching occurs, and d is the distance between dyes and the surface of metal NPs, the minimum value of which can be considered as the value of lower bound (10 nm).

The characteristic distance of d_0 can be calculated by

$$d_0 = \left(\frac{0.225 c^3 Q^0}{\omega_{donor}^2 \omega_F k_F} \right)^{1/4} \quad \text{---------- (S3)}$$

where c is the speed of light (3×10^{10} cm s^{-1}), Q^0 is the quantum yield of the dyes, ω_{donor} is the angular frequency for the donor (R123 = 3.49×10^{15} s^{-1}, S101 = 3.14×10^{15} s^{-1}), ω_F is the angular frequency for bulk silver (8.3×10^{15} s^{-1}), and k_F is the Fermi wavevector for bulk silver (1.2×10^8 cm^{-1}). [3] The quantum yields of R123 and S101 were determined as 0.43 and 0.25, respectively, by referencing dilute ethanol solutions of the same dyes. By inserting these values into Eq. (S3), the values of d_0 were determined as 6.8 nm for R123 and 6.3 nm for S101. Therefore, the efficiencies of non-radiative energy transfer could be evaluated from Eq. (S2) and were 0.17 for R123 and 0.14 for S101.

Calculation of extinction, absorption, and scattering spectra by Mie theory.

According to Mie theory, the extinction spectrum of a given metal NP can be understood in terms of absorption and scattering components and they are interconnected to fluorescence quenching and enhancement, respectively. For example, small metal NPs in the vicinity of a fluorophore usually quench its fluorescence as their extinction is mostly come from the absorption factor, while larger NPs favor fluorescence enhancement due to a superior scattering component.[4-6]

In our experiments, since NP agglomeration is not noticeable (Figure 1b) and the shape of Ag NPs is mostly spherical (Figure S2), Mie theory can be utilized to resolve the extinction spectrum of Ag NPs. To this end, we used the open-source MieCalc program.[7] By specifying the value of diameter of Ag NP (58 nm in Figure S2), the center of the extinction spectrum (454 nm in Figure S3c), and the refractive index of the medium (n = 1.59 for PS block), the extinction spectrum of Ag NPs was resolved into scattering and absorption components (Figure S5), which clearly illustrates the superior scattering component (red dashed line) compared to the absorption component (green dashed line). It would be instructive to note that the calculated extinction spectrum (solid line in Figure S5) is quite similar to the measured extinction spectrum of Ag NPs in Figure 3Sc.

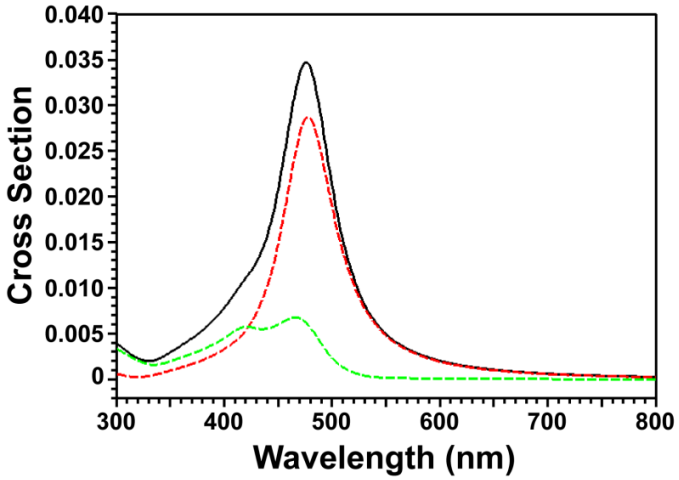

Figure S5. Calculated optical cross-section of the extinction spectrum of Ag NPs with a 58 nm diameter and a refractive index of the surrounding medium of 1.59. The extinction spectrum is the sum of the scattering component (red dashed) and absorption component (green dashed).

Dark-field optical microscopy of Ag NPs

The property of Ag NPs was further examined by a dark-field microscopy. Noticing that the dark-field image measures resonantly scattered light from Ag NPs by the surface plasmon resonance and can not be detected if NPs have dominant absorption over scattering, Figure S6 clearly confirms the strong scattering property of Ag NPs.

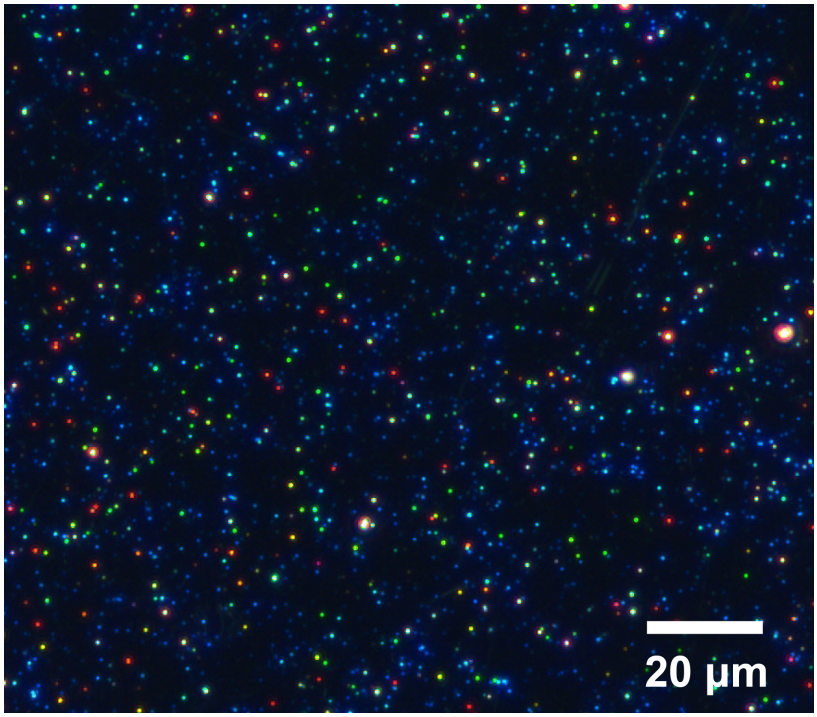

Figure S6. Dark-field scattering image of Ag NPs on the substrate. The scattering image of NP substrate was examined by a Carl Zeiss Axiovert 200 inverted microscope (Carl Zeiss, Germany) with a dark-field condenser (NA = 1.4, oil-immersion) using 40× objective lens (NA = 0.6) and with a white light illumination from a 100 W halogen lamp.

UV-Vis and fluorescence spectra of fluorescent dyes

Figure S7a is normalized UV-Vis (dashed line) and fluorescence (solid line) spectra from ethanol solutions (2.0×10^{-5} M) of R123 (green) and S101 (red), which clearly shows the spectral overlap between the emission of R123 and absorption of S101. When independently-prepared solutions of R123 and S101 were mixed at a 1:1 ratio, the fluorescence of R123 at 550 nm was substantially quenched while that of S101 at 605 nm was noticeably enhanced (violet line in Figure S7b), indicating an effective FRET from R123 (donor) to S101 (acceptor). For comparison, the fluorescence spectra from only R123 (green) and from only S101 (red) are also included.

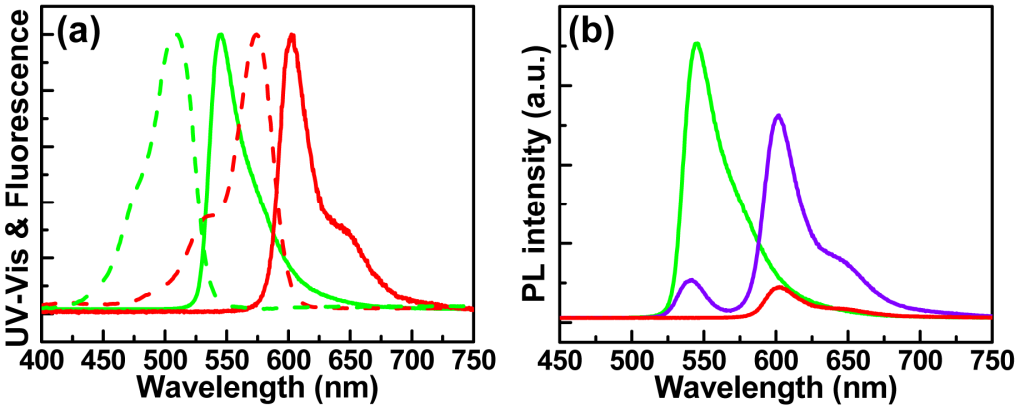

Figure S7. (a) Normalized UV-Vis (dashed line) and steady-state fluorescence (solid line) spectra from ethanol solutions of R123 (green) and S101 (red). (b) Steady-state fluorescence spectra of ethanol solutions of R123 (green), S101 (red), and mixture of R123 and S101 (purple). The excitation wavelength was 442 nm.

Further discussion on FRET (Förster radius and FRET efficiency)

If FRET occurred in the mixed micellar film in Figure 4 (main text), the lifetime of R123 in the mixed film had to be decreased in the presence of S101.[1] It appears that the separation of R123 and S101 in different micellar cores beyond their Förster radius is responsible for FRET inhibition as discussed below.

FRET efficiency (E_{FRET}) can be determined by[1]

$$E_{FRET} = R_0^6 /(R_0^6 + r^6) \text{ ---------- (S4)}$$

where R_0 is the Förster radius and r is the donor-acceptor distance. In order to understand the restricted FRET in Figure 4, we first calculated R_0 and r in the micellar system.

The Förster radius (R_0) of R123 and S101 can be calculated by[1]

$$R_0 = 0.211[k^2 n^{-4} Q_D J(\lambda)]^{1/6} \text{ ---------- (S5)}$$

where Q_D is the quantum yield of the donor (measured as 0.43), k^2 is the orientation factor (assumed as 2/3 corresponding to a random orientation), n is the refractive index of the medium (1.59 for PS blocks), and $J(\lambda)$ is the donor-acceptor overlap integral .

The overlap integral can be obtained by

$$J(\lambda) = \int_0^\infty f_D(\lambda)\varepsilon_A(\lambda)\lambda^4 d\lambda \text{ ----------(S6)}$$

where f_D is the normalized emission intensity of the donor, ε_A is the wavelength-dependent extinction coefficient of the acceptor, and λ is the wavelength in nanometer. $J(\lambda)$ was evaluated as 3.62×10^{15} M^{-1} cm^{-1} nm^4 from the absorption and fluorescence spectra of R123 and S101 in the micelles (not shown). By inserting the value of $J(\lambda)$ in Eq. (S5), R_0 was evaluated as 4.9 nm. At the same time, the donor-acceptor distance (r) in the mixed-micellar film containing R123 (donor) and S101 (acceptor) in different cores is at least the thickness of the PS coronas separating each PVP core. From Figure 1a, the thickness of the PS corona was evaluated as 20 nm. With this information, the FRET efficiency was calculated as 2.16×10^{-4} from Eq. (S4), indicating negligible FRET in the mixed-micellar film.

References

1 J. R. Lakowicz, in *Principles of Fluorescence Spectroscopy*, Kluwer Academic/Plenum, New York, 3rd edn., 2006.

2 T. L. Jennings, M. P. Singh and G. F. Strouse, *J. Am. Chem. Soc*., 2006, **128**, 5462.

3 S. Saraswat, A. Desireddy, D. Zheng, L. Guo, H. P. Lu, T. P. Bigioni and D. Isailovic, *J. Phys. Chem. C*, 2011, **115**, 17587.

4 M. Rycenga, C. M. Cobley, J. Zeng, W. Li, C. H. Moran, Q. Zhang, D. Qin and Y. Xia, *Chem. Rev.*, 2011, **111**, 3669.

5 R. Bardhan, N. K. Grady, J. R. Cole, A. Joshi and N. J. Halas, *Acs Nano*, 2009, **3**, 744.

6 J. R. Lakowicz, *Anal. Biochem*., 2005, **337**, 171.

7 C. F. Bohren and D. Huffman, MieCalc-freely configurable program for light scattering calculations (Mie theory), **2006**, http://www.lightscattering.de/MieCalc/eindex.html.